Family with sequence similarity 20 member B regulates osteogenic differentiation of bone marrow mesenchymal stem cells on titanium surfaces

Xinman Song [a], Kazuto Okabe [a,*], Yuya Ohta [b], Go Ohara [a], Naoto Toyama [b], Qi Chang [a], Yilin Wang [a], Hideharu Hibi [a,b]

[a] Department of Oral and Maxillofacial Surgery, Nagoya University Graduate School of Medicine, 65 Tsurumai-cho, Showa-ku, Nagoya, Aichi 466-8550, Japan

[b] Department of Oral and Maxillofacial Surgery, Nagoya University Hospital, 65 Tsurumai-cho, Showa-ku, Nagoya, Aichi 466-8550, Japan

*Corresponding author

Kazuto Okabe, Department of Oral and Maxillofacial Surgery, Nagoya University Graduate School of Medicine, 65 Tsurumai-cho, Showa-ku, Nagoya, Aichi 466-8550, Japan

Tel: +81-52-744-2348, Fax: +81-52-744-2352

E-mail: kokabe@med.nagoya-u.ac.jp

Abstract

Successful bone regeneration on titanium (Ti) surfaces is a key process in dental implant treatment. Bone marrow mesenchymal stem cells (BMSCs) are fundamental cellular components of this process, and their early recruitment, proliferation, and differentiation into bone-forming osteoblasts are crucial. A proteoglycan (PG)-rich layer has been reported to exist between Ti surfaces and bones; however, the molecules that could potentially affect the formation of this layer remain unknown. Family with sequence similarity 20 member B (FAM20B) is a newly identified kinase that regulates the synthesis of glycosaminoglycans, an important component of the PG-rich layer. Because FAM20B is also closely associated with bone development, in this study, we examined the function of FAM20B in osteogenic differentiation of BMSCs on Ti surfaces. For this, BMSC cell lines with knocked down FAM20B (shBMSCs) were cultured on Ti surfaces. The results showed that the depletion of FAM20B reduced the formation of a PG-rich layer between the Ti surfaces and cells. The shBMSCs exhibited downregulated expression of osteogenic marker genes (ALP and OCN) and decreased mineral deposition. Moreover, shBMSCs reduced the molecular levels of p-ERK1/2, which plays an important role in MSC osteogenesis. The nuclear translocation of RUNX2, an important transcription factor for osteogenic differentiation, on the Ti surfaces is inhibited by the depletion of FAM20B in BMSCs. Moreover, the depletion of FAM20B reduced the transcriptional activity of RUNX2, which is important in regulating the expression of osteogenic genes.

Keywords: Titanium; Osteogenesis; family with sequence similarity 20-B; Runt-related transcription factor 2

1. Introduction

Successful dental implant treatment requires bone healing and regeneration on the surfaces of implants, which are generally made of titanium (Ti) [1, 2]. Bone mesenchymal stem cells (BMSCs) play a crucial role in this process, and their early recruitment to Ti surfaces, differentiation into osteoblasts, and bone formation are essential for dental implant treatment [1, 3]. However, the underlying mechanisms of osteogenic differentiation of BMSCs on Ti surfaces have still not been elucidated.

The ultrastructures observed in numerous experiments have confirmed the existence of a proteoglycan (PG)-rich layer between the Ti surfaces and the adjacent bone [4]. The PG-rich layer has been considered to be responsible for the interfacial adhesion between bone and Ti surfaces [5]. PGs are composed of one or more glycosaminoglycan (GAG) chains that are tetrasaccharide-covalently attached to particular serine residues within a protein core[6]. Developed GAG chains are sulfated linear polysaccharides that can be further categorized as heparan sulfate or chondroitin sulfate depending on the exact composition of the extended sugar repeat sequence [6, 7]. It has been reported that the destruction of chondroitin sulfate in BMSCs results in a decreased PG-rich layer between cells and Ti surfaces [8].

A family with sequence similarity 20 member B (FAM20B) to phosphorylate xylose was found within the tetrasaccharide linkage region of PG, which significantly up regulates the activity of galactosyltransferase II, an essential enzyme for completing the linking region and glycosaminoglycan assembly. [9]. Additionally, studies have shown that knocking out FAM20B from osteosarcoma cells decreases the amounts of heparan sulfate and chondroitin sulfate on

the cell surface [9]. Many in vivo experiments have shown that FAM20B deficiency causes multiple facial defects and abnormal postnatal ossification in mice, suggesting that FAM20B plays a crucial function in the development of bones [10, 11]. In clinical cases, FAM20B deficiency has been shown to be linked with Desbuquois syndrome, in which short stature, joint laxity, and advanced carpal ossification are the main symptoms [12, 13]. However, it is still unclear how FAM20B controls the ability of BMSCs to differentiate into osteoblasts.

The osteogenic differentiation of BMSCs can be influenced by a number of signaling pathways that can be activated by the growth factors [14-18]. The osteogenic differentiation of BMSCs is distinguished by the time-dependent expression of appropriate genes [19-21]. The extracellular-regulated kinase (ERK1/2) pathway is important for maintaining bone homeostasis, and has been reported to control osteogenic differentiation in response to fibroblast growth factor 2 (FGF2) in BMSCs and affect the expression of osteoblast markers [19, 22]. Mice in which FAM20B was conditionally knocked out showed damaged intervertebral discs and altered levels of phosphorylated-ERK1/2 (p-ERK1/2) [23]. Conditional knockout of FAM20B in mouse dental epithelial cells causes alterations in the molecular amount of p-ERK1/2 and leads to the generation of multiple teeth [24]. However, the effect of FAM20B on ERK1/2 signaling in BMSCs has not yet been reported.

Runt-related transcription factor 2 (RUNX2) is the main transcription factor for osteogenesis [25-27]. It contains a DNA-binding runt domain and plays a major role in the commitment of MSCs to the osteoblastic lineage, regulating osteogenic differentiation and activating the expression of genes related to osteogenesis [25, 26]. The total absence of RUNX2 leads to

complete bone loss and perinatal death in mice, and postnatal RUNX2 deficiency leads to reduced bone mass [28, 29].

We believe that FAM20B affects the osteogenic differentiation of BMSCs via ERK1/2 and RUNX2. To test this hypothesis, we analyzed the function of FAM20B in BMSCs on Ti surfaces.

2. Materials and methods

2.1 Cell culture

UE7T-13 cell line was purchased from the Japanese Collection of Research Biosources (JCRB; Osaka, Japan), incubated with Dulbecco's modified eagle medium (DMEM) containing 10% fetal bovine serum (FBS) (Sigma-Aldrich, Tokyo, Japan) and 1% penicillin and streptomycin (PS) (Fujifilm-Wako, Osaka, Japan) at 37 °C and 5% CO_2 humidified atmosphere. HEK293 cell line was purchased from ATCC and cultured in DMEM containing 10% FBS and 1% PS.

2.2 Titanium sample generation and surface analysis

Ti plates were acquired from Ofa Co., Ltd. (Chiba, Japan) for 24-well plates and 6-well plates and 100 mm dishes. Ti foil was acquired from Nirako (Tokyo, Japan). After polishing with abrasive paper (800#), the samples were soaked in 4.0 mM HNO_3 and 0.8 mM HF and then ultrasonicated with 5% sodium dodecyl sulfate (SDS) (Fujifilm-Wako), acetone, ethanol, and distilled water. The surface morphology of the Ti samples was analyzed using high-resolution scanning electron microscopy (SEM, JSM-7610F, JEOL Ltd, Tokyo, Japan). Electron dispersive spectroscopy (EDS)

was used for compositional analysis of the Ti surfaces.

2.3 Plasmid construction

C-terminal HA-tagged RUNX2 plasmids were constructed by subcloning the RUNX2 cDNA derived from the human mosaic cDNA template (GENOFi) into pcDNA3.1-HA plasmids. The 1.5 kb OCN promoter fragment was amplified by real-time polymerase chain reaction (PCR) using mouse genomic DNA (Promega) as a template and inserted into the XhoI and HindIII sites of the pNL1.2 [NlucP] vector (Promega). To construct the p6xOSE2-Nluc reporter plasmid, which contains six tandem repeats of the osteoblast-specific core binding sequence (OSE2), oligonucleotides containing the OSE2 sequence were synthesized to create BglII and BamHI overhangs at the 5-end (Table 1). The oligonucleotides were annealed and phosphorylated with T4 polynucleotide kinase (NEB) and then cloned into the BglII site of the pNL3.2[NlucP/minP] vector (Promega) using Ligation high Ver. 2 (TOYOBO). To confirm that the 6xOSE2 multimers were tandemly repeated, the cloned plasmids were sequenced. The 6xOSE2-minP-Nluc-SV40pA cassette was amplified by PCR and inserted into the pLVX-puro lentivirus plasmid to obtain the pLVX-6xOSE2-Nluc report vector. The sequences of all plasmids were confirmed using the CEQ 8000 Genetic Analysis System (Beckman Coulter).

2.4 Establishment of stable cell lines

To generate FAM20B knockdown stable cell lines, predesigned FAM20B shRNA (Sigma-Aldrich: TRCN0000138872, TRCN0000278245) and non-target control shRNA (Sigma-Aldrich: SHC016) lentivirus plasmid vectors were co-transfected with ViraPower lentiviral packaging mix

(containing pLP1, pLP2, pVSVG plasmids, Thermo Fisher Scientific) using Lipofectamine3000 transfection reagent (Thermo Fisher Scientific) into Lenti-X 293T packaging cells (TAKARA Bio). At 48 h post-transfection, the lentivirus-containing supernatant was harvested and concentrated by ultracentrifugation at 20,000 *g* for 90 min at 4 °C. The UE7T-13 cells were infected by lentivirus with 8 μg/mL hexadimethrine bromide (Sigma) for 8 h. After two days, the UE7T-13 cells were treated with 2 μg/mL puromycin (Thermo Fisher Scientific) for three days and 1 μg/mL for 1 week (as shown in Supplementary Figure S1. The efficiency of depletion was determined using real-time PCR (RT-PCR) and western blot analyses. To establish a stable p6xOSE2-luc cell line, the HEK293 cells were infected by lentivirus for 8 h and selected using puromycin, which is consistent with the method described above with pLVX-6xOSE2-Nluc lentivirus plasmid vectors.

2.5 Real-time PCR

The cells were cultured on Ti plates for the durations indicated in the results. Subsequently, RNA was extracted using the TRIzol LS reagent (Thermo Fisher Scientific, Waltham, MA, USA). The cDNA was synthesized using ReverTra Ace qPCR RT Master Mix and gDNA remover (Toyobo Co., Ltd., Osaka, Japan), according to the manufacturer's protocol. Quantitative RT-PCR was conducted with Aria MX (Agilent, Tokyo, Japan) using the THUNDERBIRD SYBR qPCR mix (Toyobo). The expression of the target genes was compared with that of glyceraldehyde-3-phosphate dehydrogenase (GAPDH), and the relative expression of the genes to be tested was calculated using the $2^{-\Delta\Delta Ct}$ method. The sequences used for the PCR primers are shown in Table 2.

2.6 Western blotting

Proteins were harvested from cells cultured on poly and Ti for three and seven days using CelLytic M cell lysis reagent (Sigma, C2978), PhosStop (4906845001; Roche), and protease inhibitors. Nuclear and cytoplasmic extractions were performed according to the instructions of the NE-PER kit (Thermo Fisher Scientific, Waltham, MA, USA). A bicinchoninic acid (BCA) kit (UH289369; Thermo Fisher) was used according to the manufacturer's instructions to determine the protein concentration. A mixture of the protein and 6x sample buffer was separated using 10% SDS-PAGE. The mixture was transferred to a PVDF membrane at proper electricity for 1 h. The membranes were blocked with 5% nonfat milk or blocking reagent (B1210701; TOYOBO) for 1 h at room temperature. The membranes were then washed with TBS-T three times for 5 min each. Next, the membranes were incubated overnight with the following primary antibodies: FAM20B (R&D MAB8427), p44/42 MAPK(Erk1/2) (Cell Signaling 9107), p-p44/42 MAPK(p-Erk1/2) (Cell Signaling 4370), RUNX2 (Santa Cruz sc-390715), GAPDH monoclonal antibody, and peroxidase conjugated antibody (Fujifilm-Wako, 015-25473). After washing the membranes thrice with TBS-T, they were subsequently incubated with anti-rabbit IgG or anti-mouse IgG for 1 h at room temperature. Band images of immune reactions were detected with an ECL kit (GE Healthcare) and read using the ChemiDoc MP imaging system (Bio-Rad).

2.7 Cell proliferation assay

Ti plates were placed in a 24-well plate, and 2,500 cells were seeded in each well and incubated for 12, 24, 48, and 72 h. In each well, 50 μL Cell Counting Kit-8 (Dojindo Laboratories,

Kumamoto, Japan) was added, and the plate was then incubated for 1 h at 37 °C. The cell suspension was transferred to a new 96-well plate and the absorbance was tested using an Infinite 200 PRO system (Tecan Japan Co., Ltd.) at a wavelength of 450 nm.

2.8 Alizarin red staining

The Ti plates were placed in 24-well plates and seeded with 2×10^4 cells per well, and DMEM containing ascorbic acid, dexamethasone, and β-glycerophosphate. After culturing for 14 days, the cells were washed with PBS, fixed with 10% formalin for 15 min, and stained with 1% alizarin red S solution (Fujifilm-Wako) for 15 min in the dark. After staining, the cells were repeatedly rinsed with distilled water until the floating color disappeared. The mineralized nodules were dissolved by shaking with 5% formic acid for 20 min. The dissolved liquid was transferred to a 96-well plate and absorbance was measured at a wavelength of 450 nm using an Infinite 200 PRO system (Tecan Japan Co., Ltd.).

2.9 Immunofluorescence (IF)

The cells were grown on Ti plates, rinsed in PBS, fixed with ice-cold 4% paraformaldehyde, and permeabilized with 0.2% Triton X-100 in PBS. The cells were then incubated with Blocking One Histo (Nacalai Tesque Inc., Kyoto, Japan) for 10 min. Primary antibodies were applied overnight at 4 °C. The primary antibodies used were anti-FAM20B (1:1000; HPA007409; Sigma), anti-vinculin (1:250; ab129002; Abcam), and anti-RUNX2 (1:250; sc-390715; Santa Cruz Biotechnology). Goat anti-rabbit IgG (H+L) highly cross-adsorbed secondary antibody and Alexa Fluor 546 (1:500; A11035; Thermo Fisher Scientific) were then applied and kept for 1 h at room

temperature. The cells were counterstained with Actin-stain 488 phalloidin (1:500; Cytoskeleton Inc. Co; Denver, CO, USA) for 1 h. Finally, the samples were sealed with a DAPI containing sealer (Vector Laboratories, Inc., Burlingame, CA, USA) and observed with a BZ-X810 all-in-one fluorescence microscope (Keyence, Osaka, Japan).

2.10 Transmission electron microscopy

The cells were cultivated on a Ti foil for 14 days. Subsequently, the cells were fixed with a solution of 4% paraformaldehyde, 2% glutaraldehyde, and 0.1 M sodium cacodylate overnight at 4 °C. The cells were then rinsed with ice-cold 0.1 M sodium cacodylate buffer. Then, the cells were stained with ruthenium red (10 mg/mL) for one hour at room temperature. A mixture of OsO_4 and ruthenium red was used for secondary fixation and re-staining for 1 h. This was followed by gradient dehydration and replacement with alcohol or propylene oxide. The samples were embedded in EPON resin (Nisshin EM Co. Ltd., Tokyo, Japan) and placed in a desiccator for 48 h. After the samples were cured, the Ti foils were removed, and secondary resin embedding was performed. The samples were ultrasonically sectioned using an ultramicrotome (EM UC7i, Leica, Tokyo, Japan), stained with lead citrate for 7s, and observed using a transmission electron microscope (JEM-1400PLUS, JEOL).

2.11 Alkaline phosphatase assay and alkaline phosphatase staining

Ti plates were placed in 24-well plates, and each well was seeded with 2×10^4 cells per week. Alkaline phosphatase assay (LabAssay ALP kit, Fujifilm-Wako) and alkaline phosphatase staining (TRAP/ALP kit, Fujifilm-Wako, Japan) were carried out according to the manufacturer's

instructions.

2.12 Reporter assay

MISSION FAM20B siRNA1(SASI_Hs02_00346448), siRNA2(SASI_Hs01_00210460) and MISSION siRNA Universal Negative Control (SIC001) were obtained from Sigma-Aldrich. The target sequences for FAM20B were 5′- ACCGCCAUCACUAUGAGAG-3′ and 5′-CUUUCACUUGGACAGGAUU-3′. To determine the RUNX2 transcription activity, RUNT DNA-binding consensus sequences 5′-ACCACA-3′ (OSE2) and OCN-promoter based luciferase reporter assay were designed. p6xOSE2-Luc cells containing a luciferase reporter gene and six tandem OSE2 were seeded in 24-well plates and co-transfected with 100 nM of FAM20B-siRNA or control siRNA with pGL4.54[luc2/TK] plasmid using a Lipofectamine 3000 transfection reagent (Thermo Fisher Scientific). HEK293 cells were seeded in 24-well plates and co-transfected with 100 nM of FAM20B-siRNA or control siRNA, pcDNA3.1-RUNX2-HA or control pcDNA3.1 plasmid with pNL1.2 [Nluc] /Bglp promoter and pGL4.54[luc2/TK] plasmid using a Lipofectamine 3000 transfection reagent. After 72 h, the cell lysates were prepared using passive lysis buffer (Promega), and the NanoLuc luminescence was measured using a Nano-Glo Dual-Luciferase Reporter Assay System (Promega) according to the manufacturer's instructions (as shown in Supplementary Figure S2.

2.13 Statistical analysis

Western blotting, transmission electron microscopy, and Immunofluorescence were analyzed using the ImageJ software. Statistics were examined utilizing one-way analysis of variance

(ANOVA), two-way ANOVA, or T test using GraphPad Prism8. *p < 0.05, **p < 0.01 were considered statistically significant.

3. Results

3.1 Topology of Ti surface

Figure 1A shows the morphology of the treated Ti surfaces (machined surfaces with ridges and valleys along the treating direction) as observed through SEM. Herein, it can be observed that the surfaces were clean and devoid of any contamination. Figure 1B shows the elemental composition of the treated Ti surfaces as obtained through EDS.

3.2 Establishing FAM20B knockdown cell lines

To investigate the role of FAM20B in osteogenesis, we obtained stable UE7T-13 cell lines wherein FAM20B was knocked down. Two shRNA sequences and one control were separately inserted into the UE7T-13 cell line using a lentivirus system. Knockdown efficiency was determined by RT-PCR, western blotting, and IF using relative mRNA and protein expression. The results of RT-PCR, western blotting, and IF showed effective lower FAM20B expression in FAM20B shRNA-1 BMSCs and FAM20B shRNA-2 BMSCs (sh groups) compared to normal BMSCs and control shRNA BMSCs (control groups) (Figure 1C–E). Furthermore, the cell proliferation tests revealed that the depletion of FAM20B increased cell proliferation after the cells were cultured on Ti surfaces for 48 h (Figure 1F).

3.3 Effect of FAM20B on focal adhesion and PG-rich layer of BMSCs cultured on Ti

surfaces

The initial cell adhesion and final focal adhesion of BMSCs to Ti surfaces were analyzed by staining vinculin. Quantification of the vinculin was done 1, 2, and 24 h after culturing the cells on Ti surfaces, and the results are shown in Figures 2A and 2B. Herein, it can be observed that sh groups showed no significant difference in the area of expression of vinculin from the control group at any time. Transmission electron microscopy was used to image the PG-rich layer, and after 14 days of culture, the area of the PG-rich layer on the interface was observed to be lower in the sh groups than in the control group (Figure 2C, D).

3.4 Effect of FAM20B on osteogenic differentiation of BMSCs cultured on Ti surfaces

The cells were cultured on Ti surfaces for seven days. Expression of osteogenic biomarkers ALP and OCN was downregulated in sh groups. However, the expression of RUNX2 did not show a difference in all groups (Figure 3A). ALP staining was lighter in the sh groups. Similarly, ALP activity also decreased in the sh groups after culturing on Ti surfaces for seven days (Figure 4A, B). Cells were subsequently incubated on Ti surfaces with osteogenic induction medium for 14 days, and alizarin red staining was applied to investigate the effect of FAM20B on the mineralization of BMSCs. As shown in (Figure 4C), lower calcified nodules were observed in sh groups.

3.5 Effect of FAM20B on activation of ERK1/2 signaling of BMSCs cultured on Ti surfaces

Cells were cultured on Ti surfaces for three days. The results of western blotting showed that pERK1/2 expression levels in the sh groups were lower than that in the control group while

maintaining the values for total ERK1/2 (Figure 4D, E). The ERK1/2 activation by FGF2 in BMSCs stimulates osteogenic gene expression. Therefore, the control and sh groups were all treated with or without recombinant human FGF2 (10 ng/mL) for an extra 6 h in serum-free medium after all cell groups had been grown on Ti surfaces overnight in a medium containing 10% FBS. In comparison to no FGF2 administration, FGF2 treatment promoted ALP expression in all groups, but the level of enhancement was higher in the control group than in the sh group. Treatment with FGF2 increased the OCN expression in the control group but not in the sh groups (Figure 3B).

3.6 Effect of FAM20B on RUNX2 nuclear translocation

The effect of FAM20B on nuclear translocation of RUNX2 in the osteogenic differentiation of BMSCs was also investigated by IF and Western blotting. IF tests showed that while majority of the RUNX2 was in the nucleus for the control group, it was in the cytosol for the sh groups when the cells were cultured on Ti surfaces for 24 h and 72 h (Figure 5A, B). Likewise, the results of western blotting tests showed that the sh groups exhibited decreased RUNX2 in the nucleus and increased RUNX2 in the cytosol when the cells were cultured on Ti surfaces for 24 h and 72 h, but their total RUNX2 amount was similar to that of the control group (Figure 5 C, D).

3.7 Effect of FAM20B on RUNX2 transcriptional activity

Luciferase reporter assay was performed to verify whether the transcriptional activity of RUNX2 was altered after depletion of FAM20B. Reporter assays were performed based on the activation of the Runt DNA-binding consensus sequence 5′-ACCACA-3′ (OSE2) in the absence

or presence of FAM20B siRNA. Efficiency of FAM20B siRNA was determined by western blotting relative to protein expression, downregulated expression of FAM20B are shown in Figure 6A. As can be observed in Figure 6B, transcriptional activity decreased in FAM20B siRNA groups compared to the control group. To further explore the regulation of RUNX2 transactivation by FAM20B, we established an OCN promoter-based luciferase reporter plasmid and performed reporter assays to investigate whether depletion of FAM20B could influence activation of the OCN promoter regulated by RUNX2. We found that the RUNX2-promoted activation of the OCN promoter was significantly decreased by depletion of FAM20B (Figure 6C).

4. **Discussion**

In this study, we established BMSC cell lines devoid of FAM20B and analyzed their function in the osteogenic differentiation of BMSCs on Ti surfaces. After culturing for 14 days on Ti surfaces, a reduced PG-rich layer was observed between the cells and the surfaces, which was probably because of the incomplete formation of GAGs as a result of FAM20B depletion. Because chondroitin sulfate was reported to be a major component of the PG-rich layer [30]. Although the depletion of FAM20B affects the formation of GAGs, it does not affect the secretion of PGs [9]. Syndecan, which is rich in heparan sulfate and is present on the cell surface, is responsible for generating signals to regulate focal adhesion. Vinculin expression in osteoblasts on the titanium surface was unaffected even by Syndecan depletion [31]. Therefore, focal adhesion was not altered by the decrease in GAGs caused by FAM20B depletion.

We also found that FAM20B depletion (a) resulted in decreased expression of osteogenesis-related factors, (b) decreased ALP formation capacity and activity, and (c) reduced mineralization

ability in BMSCs cultured on Ti surfaces. These results suggest that FAM20B is an essential component for osteogenic differentiation of BMSCs cultured on Ti surfaces. In addition, depletion of FAM20B resulted in a reduced molecular level of pERK after FGF2 treatment. This further suggests that depletion of FAM20B inhibits the activation of the ERK1/2 signaling pathway. A previous study had also shown that Biglycan, one of the proteoglycans in the extracellular matrix of bone, plays a crucial part in bone formation, activating the ERK1/2 signaling pathway to promote osteoblast differentiation and matrix mineralization, in which GAG chains played an important role [32]. Moreover, heparan sulfate promotes the binding of FGF2 to its receptors (FGF2R), thereby enhancing osteoblast differentiation [33-35]. Therefore, the decrease in GAGs caused by the depletion of FAM20B may be one of the reasons for the reduced osteogenic differentiation of BMSCs. Interestingly, the proliferation rate of the FAM20B depleted cells was relatively faster after 48 h of incubation on the Ti surface. The osteogenic process has three stages: proliferation, maturation of the extracellular matrix, and mineralization. The proliferative phase is inhibited the earliest to induce the maturation stage, while maturation and mineralization have similar transitional processes [28]. Therefore, the relative increase in the cell proliferation rate after 48 h could be due to the inhibition of the proliferation-to-maturation phase transition.

In the present study, depletion of FAM20B was observed to inhibit the osteogenic differentiation of BMSCs cultured on Ti surfaces, even though the expression of RUNX2 remained unchanged. As a mechanism, the results of IF and Western blotting showed that depletion of FAM20B in BMSCs inhibited nuclear translocation of RUNX2 and reduced its transcriptional activity. STAT1, a negative regulator of bone formation, interacted within the

cytoplasm and inhibited the nuclear localization of RUNX2. It then reduced osteoblast differentiation by decreasing transcriptional activity, resulting in decreased alkaline phosphatase activity and loss of mineralized nodules, but it did not affect RUNX2 expression [36]. As soluble heparin-like GAGs are reported to block STAT1 upregulation by IFN-γ [37], we hypothesized that the decrease in GAGs due to depletion of FAM20B may be responsible for the inhibition of nuclear localization of RUNX2 via STAT-1 and a decrease in its transcriptional activity. That said, further studies on the relationship between FAM20B and STAT-1 are required. Regarding the relationship between ERK activation and RUNX2, ERK has been reported to not affect gene expression but stimulate transcriptional activity [38]. p-ERK phosphorylates RUNX2 at its target sites (Ser-301 and Ser-319) [39]. Phosphorylation at the Ser-301 site induces subsequent acetylation of RUNX2 and regulates its transcriptional activity. The phosphorylation of RUNX2 also maintains RUNX2 stability by regulating RUNX2 ubiquitination in an ERK-dependent manner [40]. The depletion of FAM20B was observed to reduce pERK1/2 signaling; this may have directly led to a decrease in transcriptional activity.

Although this study focused on BMSCs, they are not sufficient for successful dental implant treatment. Cell-to-cell communication is important physiological processes for bone healing [1, 3]. Blood vessel formation stimulates bone formation [41]. It has been shown that most pro-angiogenic factors required for endothelial cell proliferation and migration (e.g., vascular endothelial growth factor and FGF2) bind to the sugar moieties of the heparan sulfate proteoglycan in the cell membrane and extracellular matrix [42]. Blood vessel formation is generated by endothelial cell proliferation and differentiation [43], and the role of FAM20B in the

biological activity of endothelial cells must be explored. To summarize, in this study, a part of the mechanism of bone formation on Ti surfaces has been elucidated, which is the primary focus of dental implant therapy. Further research on FAM20B is required for discovering a drug that will ensure successful dental implant treatment.

5. Conclusion

This study showed that FAM20B affected the osteogenic differentiation of BMSCs on Ti surfaces through ERK1/2 and RUNX2 transcriptional activity.

Funding

This work was supported by the JSPS KAKENHI (Grant Number: JP19K10264). The funder had no role in the study design; in the collection, analysis, and interpretation of data; in the writing of the report; or in the decision to submit the article for publication.

References

[1] X. Wang, F.A. Shah, F. Vazirisani, A. Johansson, A. Palmquist, O. Omar, K. Ekstrom, P. Thomsen, Exosomes influence the behavior of human mesenchymal stem cells on titanium surfaces, Biomaterials 230 (2020) 119571.

[2] J. Cui, L. Xia, K. Lin, X. Wang, In situ construction of a nano-structured akermanite coating for promoting bone formation and osseointegration of Ti-6Al-4V implants in a rabbit osteoporosis model, J Mater Chem B 9(46) (2021) 9505-9513.

[3] K.M. Hotchkiss, N.M. Clark, R. Olivares-Navarrete, Macrophage response to hydrophilic biomaterials regulates MSC recruitment and T-helper cell populations, Biomaterials 182 (2018) 202-215.

[4] L. Linder, T. Albrektsson, P.I. Branemark, H.A. Hansson, B. Ivarsson, U. Jonsson, I. Lundstrom, Electron microscopic analysis of the bone-titanium interface, Acta Orthop Scand 54(1) (1983) 45-52.

[5] H. Nakamura, J. Shim, F. Butz, H. Aita, V. Gupta, T. Ogawa, Glycosaminoglycan degradation reduces mineralized tissue-titanium interfacial strength, J Biomed Mater Res A 77(3) (2006) 478-86.

[6] K. Prydz, K.T. Dalen, Synthesis and sorting of proteoglycans, Journal of Cell Science 113(2) (2000) 193-205.

[7] S. Sarrazin, W.C. Lamanna, J.D. Esko, Heparan sulfate proteoglycans, Cold Spring Harb Perspect Biol 3(7) (2011).

[8] H. Kamio, S. Tsuchiya, K. Kuroda, M. Okido, K. Okabe, Y. Ohta, N. Toyama, H. Hibi, Chondroitin-4-sulfate transferase-1 depletion inhibits formation of a proteoglycan-rich layer and alters immunotolerance of bone marrow mesenchymal stem cells on titanium oxide surfaces, Acta Biomater 114 (2020) 460-470.

[9] J. Wen, J. Xiao, M. Rahdar, B.P. Choudhury, J. Cui, G.S. Taylor, J.D. Esko, J.E. Dixon, Xylose phosphorylation functions as a molecular switch to regulate proteoglycan biosynthesis, Proc Natl Acad Sci U S A 111(44) (2014) 15723-8.

[10] X. Liu, N. Li, H. Zhang, J. Liu, N. Zhou, C. Ran, X. Chen, Y. Lu, X. Wang, C. Qin, J. Xiao, C. Liu, Inactivation of Fam20b in the neural crest-derived mesenchyme of mouse causes multiple craniofacial defects, Eur J Oral Sci 126(5) (2018) 433-436.

[11] P. Ma, W. Yan, Y. Tian, J. Wang, J.Q. Feng, C. Qin, Y.S. Cheng, X. Wang, Inactivation of Fam20B in Joint Cartilage Leads to Chondrosarcoma and Postnatal Ossification Defects, Sci Rep 6 (2016) 29814.

[12] C. Bui, C. Huber, B. Tuysuz, Y. Alanay, C. Bole-Feysot, J.G. Leroy, G. Mortier, P. Nitschke, A. Munnich, V. Cormier-Daire, XYLT1 mutations in Desbuquois dysplasia type 2, Am J Hum Genet 94(3) (2014) 405-14.

[13] Y. Kuroda, H. Murakami, Y. Enomoto, Y. Tsurusaki, K. Takahashi, K. Mitsuzuka, H. Ishimoto, G. Nishimura, K. Kurosawa, A novel gene (FAM20B encoding glycosaminoglycan xylosylkinase) for neonatal short limb dysplasia resembling Desbuquois dysplasia, Clin Genet 95(6) (2019) 713-717.

[14] K. Hanada, J.E. Dennis, A.I. Caplan, Stimulatory Effects of Basic Fibroblast Growth Factor and Bone Morphogenetic Protein-2 on Osteogenic Differentiation of Rat Bone Marrow-Derived Mesenchymal Stem Cells, Journal of Bone and Mineral Research 12(10) (1997) 1606-1614.

[15] F. Gori, T. Thomas, K.C. Hicok, T.C. Spelsberg, B.L. Riggs, Differentiation of Human Marrow

Stromal Precursor Cells: Bone Morphogenetic Protein-2 Increases OSF2/CBFA1, Enhances Osteoblast Commitment, and Inhibits Late Adipocyte Maturation, Journal of Bone and Mineral Research 14(9) (1999) 1522-1535.
[16] S.L. Etheridge, G.J. Spencer, D.J. Heath, P.G. Genever, Expression Profiling and Functional Analysis of Wnt Signaling Mechanisms in Mesenchymal Stem Cells, Stem Cells 22(5) (2004) 849-860.
[17] T. Gaur, C.J. Lengner, H. Hovhannisyan, R.A. Bhat, P.V. Bodine, B.S. Komm, A. Javed, A.J. van Wijnen, J.L. Stein, G.S. Stein, J.B. Lian, Canonical WNT signaling promotes osteogenesis by directly stimulating Runx2 gene expression, J Biol Chem 280(39) (2005) 33132-40.
[18] A.M. Osyczka, P.S. Leboy, Bone Morphogenetic Protein Regulation of Early Osteoblast Genes in Human Marrow Stromal Cells Is Mediated by Extracellular Signal-Regulated Kinase and Phosphatidylinositol 3-Kinase Signaling, Endocrinology 146(8) (2005) 3428-3437.
[19] H. Miraoui, K. Oudina, H. Petite, Y. Tanimoto, K. Moriyama, P.J. Marie, Fibroblast growth factor receptor 2 promotes osteogenic differentiation in mesenchymal cells via ERK1/2 and protein kinase C signaling, J Biol Chem 284(8) (2009) 4897-904.
[20] J. Zhang, W. Zhang, J. Dai, X. Wang, S.G. Shen, Overexpression of Dlx2 enhances osteogenic differentiation of BMSCs and MC3T3-E1 cells via direct upregulation of Osteocalcin and Alp, Int J Oral Sci 11(2) (2019) 12.
[21] G. Karsenty, Role of Cbfa1 in osteoblast differentiation and function, Semin Cell Dev Biol 11(4) (2000) 301-8.
[22] H.J. Kim, M.H. Lee, H.S. Park, M.H. Park, S.W. Lee, S.Y. Kim, J.Y. Choi, H.I. Shin, H.J. Kim, H.M. Ryoo, Erk pathway and activator protein 1 play crucial roles in FGF2-stimulated premature cranial suture closure, Dev Dyn 227(3) (2003) 335-46.
[23] W. Saiyin, L. Li, H. Zhang, Y. Lu, C. Qin, Inactivation of FAM20B causes cell fate changes in annulus fibrosus of mouse intervertebral disc and disc defects via the alterations of TGF-beta and MAPK signaling pathways, Biochim Biophys Acta Mol Basis Dis 1865(12) (2019) 165555.
[24] Y. Tian, P. Ma, C. Liu, X. Yang, D.M. Crawford, W. Yan, D. Bai, C. Qin, X. Wang, Inactivation of Fam20B in the dental epithelium of mice leads to supernumerary incisors, Eur J Oral Sci 123(6) (2015) 396-402.
[25] T. Komori, Runx2, a multifunctional transcription factor in skeletal development, J Cell Biochem 87(1) (2002) 1-8.
[26] T. Komori, Regulation of skeletal development by the Runx family of transcription factors, J Cell Biochem 95(3) (2005) 445-53.
[27] F. Long, Building strong bones: molecular regulation of the osteoblast lineage, Nat Rev Mol Cell Biol 13(1) (2011) 27-38.
[28] S. Vimalraj, B. Arumugam, P.J. Miranda, N. Selvamurugan, Runx2: Structure, function, and phosphorylation in osteoblast differentiation, Int J Biol Macromol 78 (2015) 202-8.
[29] I. Tosa, D. Yamada, M. Yasumatsu, E. Hinoi, M. Ono, T. Oohashi, T. Kuboki, T. Takarada, Postnatal Runx2 deletion leads to low bone mass and adipocyte accumulation in mice bone tissues, Biochem Biophys Res Commun 516(4) (2019) 1229-1233.
[30] M M Klinger, F Rahemtulla, C W Prince, L C Lucas, J E Lemons Crit Rev Oral Biol Med 9(4) (1998) 449-63.
[31] L. Sun, G. Hong, H. Matsui, Y.J. Song, K. Sasaki, The Effects of Syndecan on Osteoblastic Cell

Adhesion Onto Nano-Zirconia Surface, Int J Nanomedicine 15 (2020) 5061-5072.
[32] X. Wang, K. Harimoto, S. Xie, H. Cheng, J. Liu, Z. Wang, Matrix Protein Biglycan Induces Osteoblast Differentiation through Extracellular Signal-Regulated Kinase and Smad Pathways, Biological and Pharmaceutical Bulletin 33(11) (2010) 1891-1897.
[33] S. Guimond, M. Maccarana, B.B. Olwin, U. Lindahl, A.C. Rapraeger, Activating and inhibitory heparin sequences for FGF-2 (basic FGF). Distinct requirements for FGF-1, FGF-2, and FGF-4, Journal of Biological Chemistry 268(32) (1993) 23906-23914.
[34] J. Chen, T. Sun, Y. You, B. Wu, X. Wang, J. Wu, Proteoglycans and Glycosaminoglycans in Stem Cell Homeostasis and Bone Tissue Regeneration, Front Cell Dev Biol 9 (2021) 760532.
[35] L. Ling, C. Dombrowski, K.M. Foong, L.M. Haupt, G.S. Stein, V. Nurcombe, A.J. van Wijnen, S.M. Cool, Synergism between Wnt3a and heparin enhances osteogenesis via a phosphoinositide 3-kinase/Akt/RUNX2 pathway, J Biol Chem 285(34) (2010) 26233-44.
[36] S. Kim, T. Koga, M. Isobe, B.E. Kern, T. Yokochi, Y.E. Chin, G. Karsenty, T. Taniguchi, H. Takayanagi, Stat1 functions as a cytoplasmic attenuator of Runx2 in the transcriptional program of osteoblast differentiation, Genes Dev 17(16) (2003) 1979-91.
[37] M.S. Douglas, S. Ali, D.A. Rix, J.G. Zhang, J.A. Kirby, Endothelial production of MCP-1: modulation by heparin and consequences for mononuclear cell activation, Immunology 92(4) (1997) 512-8.
[38] G. Xiao, D. Jiang, R. Gopalakrishnan, R.T. Franceschi, Fibroblast growth factor 2 induction of the osteocalcin gene requires MAPK activity and phosphorylation of the osteoblast transcription factor, Cbfa1/Runx2, J Biol Chem 277(39) (2002) 36181-7.
[39] C. Ge, G. Xiao, D. Jiang, Q. Yang, N.E. Hatch, H. Roca, R.T. Franceschi, Identification and functional characterization of ERK/MAPK phosphorylation sites in the Runx2 transcription factor, J Biol Chem 284(47) (2009) 32533-43.
[40] O.J. Park, H.J. Kim, K.M. Woo, J.H. Baek, H.M. Ryoo, FGF2-activated ERK mitogen-activated protein kinase enhances Runx2 acetylation and stabilization, J Biol Chem 285(6) (2010) 3568-3574.
[41] Y. Qin, R. Sun, C. Wu, L. Wang, C. Zhang, Exosome: A Novel Approach to Stimulate Bone Regeneration through Regulation of Osteogenesis and Angiogenesis, Int J Mol Sci 17(5) (2016).
[42] X.M. van Wijk, T.H. van Kuppevelt, Heparan sulfate in angiogenesis: a target for therapy, Angiogenesis 17(3) (2014) 443-62.
[43] C.J. Percival, J.T. Richtsmeier, Angiogenesis and intramembranous osteogenesis, Dev Dyn 242(8) (2013) 909-22.

Table 1. Primer sequences for plasmids used in this study.

Plasmids	Sequence of oligomers
pcDNA3.1-RUNX2-HA	F: TGGAATTCTGCAGATATCCACCATGGCATCAAACAGC
	R: GTATGGGTATCTCGAGCAATATGGTCGCCAAACAGATTC
pNL1.2-OCN-promoter	F: GCTCGCTAGCCTCGAGCCTTTCCAGCCTTAATCTGTGACG
	R: CCGGATTGCCAAGCTTATGGTGTCTGCTAGGTCTGGG
pNL3.2-6xOSE2-minP	F: GATCTAGCTGCAATCACCAACCACAGCATGR:
	R: GATCCATGCTGTGGTTGGTGATTGCAGCTA
pLVX-puro-6xORE2-minP	F: AGATCCAGTTTATCGATGGCCTAACTGGCCGGTACC
	R: TAGAGTCGCGGGATCCTTTACCACATTTGTAGAGG

Table 2. Primer sequences for q-PCR.

Genes	Sequence (forward5$^{'}$ – 3$^{'}$)	Sequence (reverse3$^{'}$ – 5$^{'}$)
GAPD	AGCAAGAGCACAAGAGGAA	TCTACATGGCAACTGTGAG
FAM2	GCTGTTGAGCACCTTCCTA	ATGTCTCCATCAGCACAAG
ALP	AGCTGAACAGGAACAACGT	ATTCTGCCTCCTTCCACCA
OCN	CACACTCCTCGCCCTATTG	CGCCTGGGTCTCTTCACTA
OSX	GAGGCAACTGGCTAGGTG	CTGGATTAAGGGGAGCAAA

Abbreviations: ALP, Alkaline phosphatase; OCN, osteocalcin; OSX, osterix.

Figure captions

Figure 1

(A) SEM images showing Ti surface characteristics after treatment at 100× and 1,000× magnifications. (B) Elemental analysis of Ti surfaces. Abbreviations: C, carbon; N, nitrogen; O, oxygen; F, fluorine; Al, aluminum; Si, silicon; Ti, titanium; V, vanadium; Cu, copper. (C) Established FAM20B knockdown UE7T-13 cell lines. Changes in FAM20B mRNA expression determined using RT-PCR. (D) FAM20B protein levels measured by western blot analysis. (E) Immunofluorescence of FAM20B in Normal, Control and sh groups after culturing on Ti surfaces for 24 h. Scale bar: 80 μm. (F) Cell proliferation of BMSCs on Ti surfaces. Three independent experiments were performed, data are shown as the mean ± S.E. (*, $p < 0.05$, **, $p < 0.01$)

Figure 2

Focal adhesion and PG-rich layer formation in control and sh BMSCs on Ti surfaces. (A) Immunofluorescence of vinculin (red) actin (green) and DAPI (blue) after 1 h, 2h, and 24 h. (B) quantification of vinculin positive area. (C) Transmission electron micrographs of interface between BMSCs and Ti surfaces; the PG-rich layer stained intensely with ruthenium red is indicated by the black arrows. (D) Quantification of PG-rich layer area. PG-rich layer reduced in sh groups. Scale bar: 600 nm. Three samples were prepared for each experimental group, and fifteen images were analyzed for each experimental group. *$p<0.05$.

Figure 3

Osteogenic differentiation capacity of control and FAM20B shRNA BMSCs on Ti surfaces. (A) Gene expression of the osteogenic biomarkers ALP, OCN, and RUNX2 of BMSCs on Ti surfaces. (B) Gene expression of the osteogenic biomarkers ALP and OCN of BMSCs on Ti surfaces after 6 h of FGF2 stimulation. Three independent experiments were performed, data are shown as the mean ± S.E. (*, $p < 0.05$, **, $p < 0.01$.)

Figure 4

ALP activity and mineralization capacity of control and FAM20B shRNA BMSCs on Ti surfaces. (A) Representative images of ALP staining of BMSCs on Ti surfaces. (B) Quantitative analysis of ALP activity assay. (C) Representative images of alizarin red S staining of BMSCs on Ti surfaces and quantitative analysis of calcified nodules. Activation of ERK1/2 in control and FAM20B shRNA BMSCs on Ti surfaces. (D) Protein levels of the pERK1/2 in BMSCs on Ti surfaces as revealed by western blotting. (E) Quantification of signal intensities. Three independent experiments were performed, data are shown as the mean ± S.E. (*, $p < 0.05$, **, $p < 0.01$)

Figure 5

RUNX2 nuclear localization in control and FAM20B shRNA BMSCs on Ti surfaces. (A, B) Distribution of RUNX2 of BMSCs on Ti surfaces. Red is RUNX2 and blue is DAPI. (C, D) Western blotting results showed RUNX2 expression in nuclear (N) extracts, cytosol (C) extracts, and total proteins. TBP (TATA-binding protein) and α-tubulin as a loading control for nuclear and cytosolic

fractions. Three independent experiments were performed; data represented as mean ± S.E. (*, $p < 0.05$, **, $p < 0.01$)

Figure 6

Transcriptional activity of RUNX2 in control and FAM20B siRNA HEK293 cell line. (A) Western blotting results of FAM20B siRNA efficiency. (B) OSE2-dependent luciferase activity (C) OCN promoter-dependent luciferase activity. Three independent experiments were performed, data are shown as the mean ± S.E. (*, $p < 0.05$, **, $p < 0.01$)

Figure 1

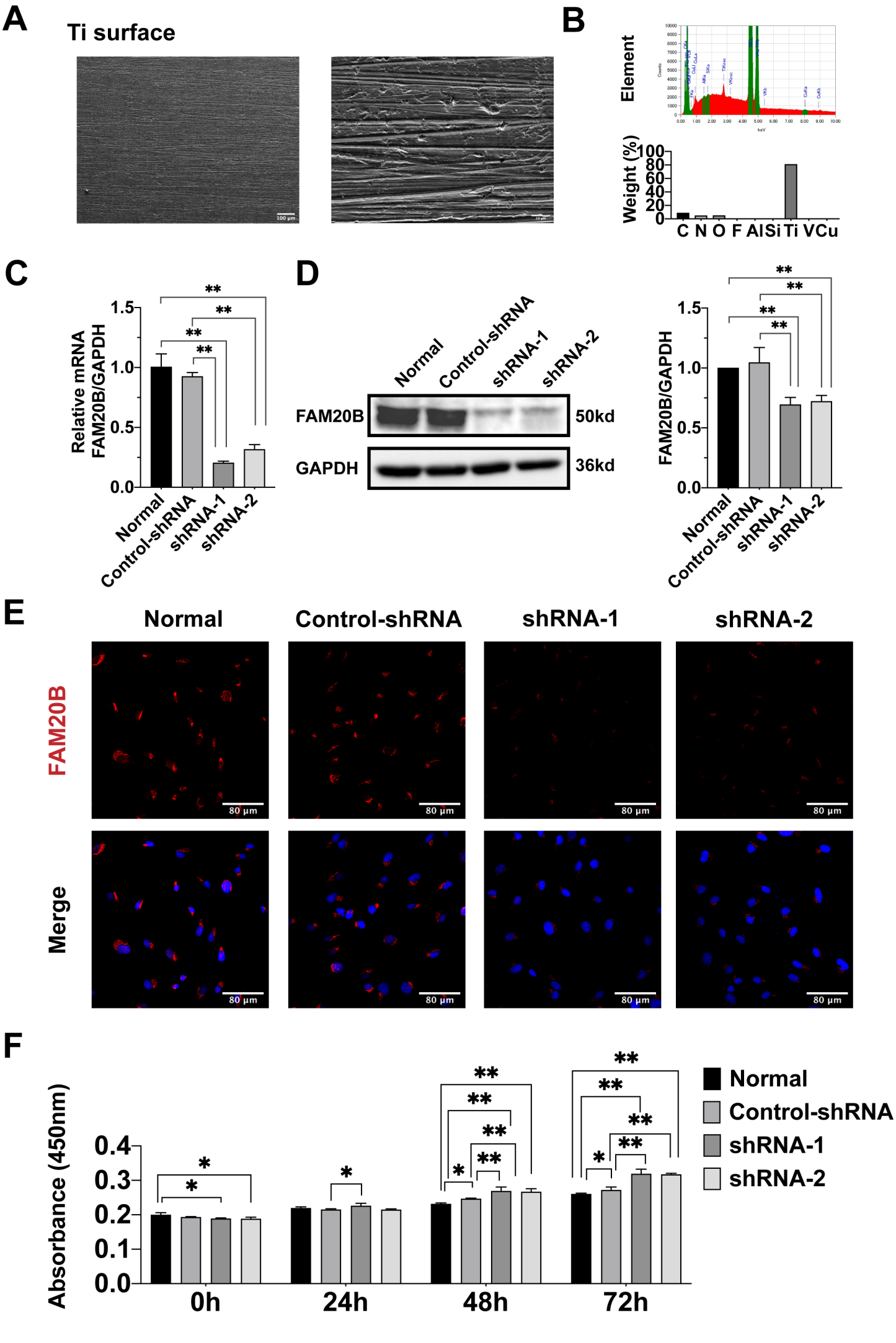
A
Ti surface
B
Element
Weight (%)
C N O F Al Si Ti V Cu
C
Relative mRNA FAM20B/GAPDH
Normal
Control-shRNA
shRNA-1
shRNA-2
D
FAM20B
GAPDH
50kd
36kd
FAM20B/GAPDH
E
FAM20B
Merge
80 μm
F
Absorbance (450nm)
0h
24h
48h
72h

Figure 2

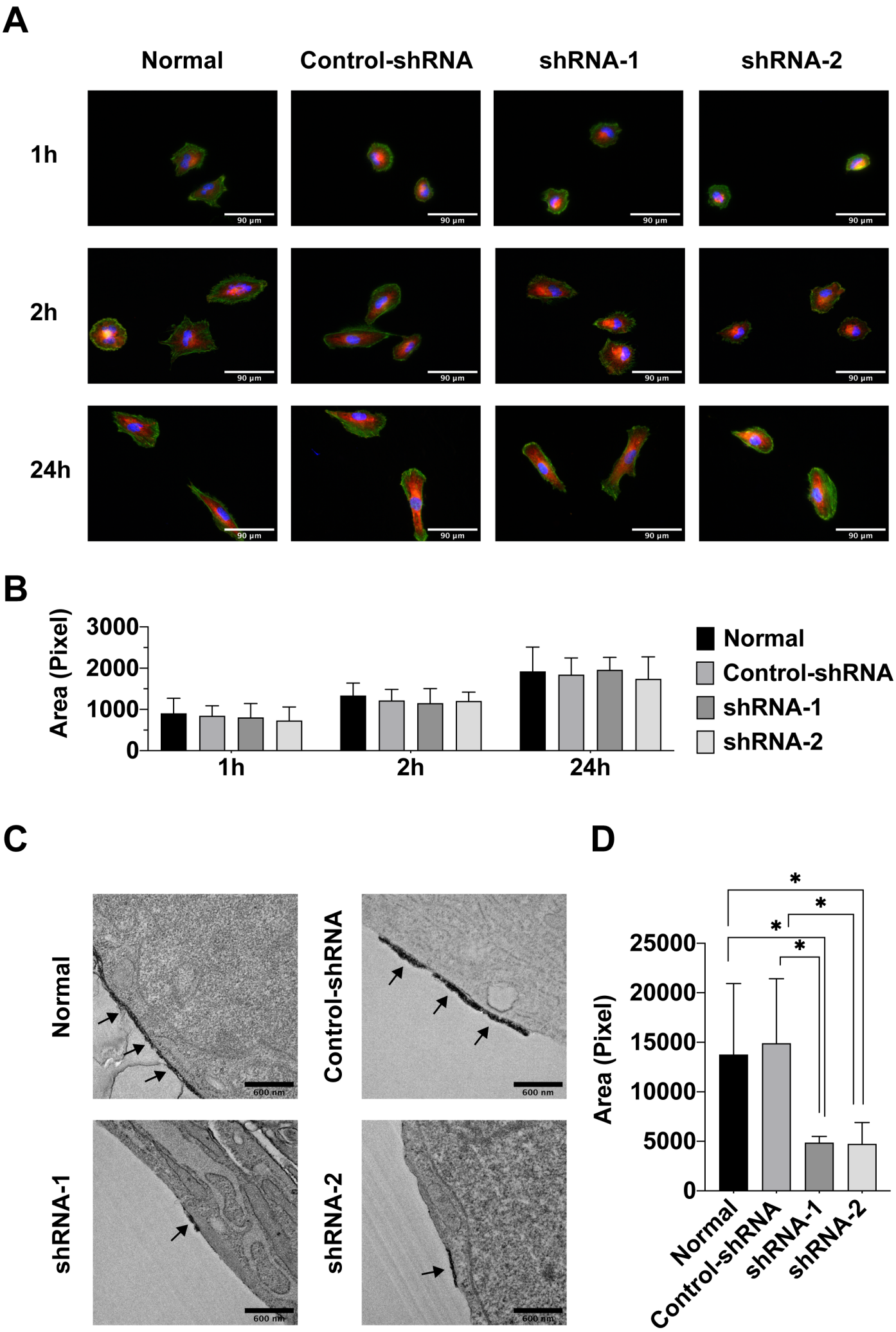
A
Normal
Control-shRNA
shRNA-1
shRNA-2
1h
2h
24h
90 μm
B
Area (Pixel)
3000
2000
1000
0
1h
2h
24h
Normal
Control-shRNA
shRNA-1
shRNA-2
C
Normal
Control-shRNA
shRNA-1
shRNA-2
600 nm
D
Area (Pixel)
25000
20000
15000
10000
5000
0
*
Normal
Control-shRNA
shRNA-1
shRNA-2

Figure 3

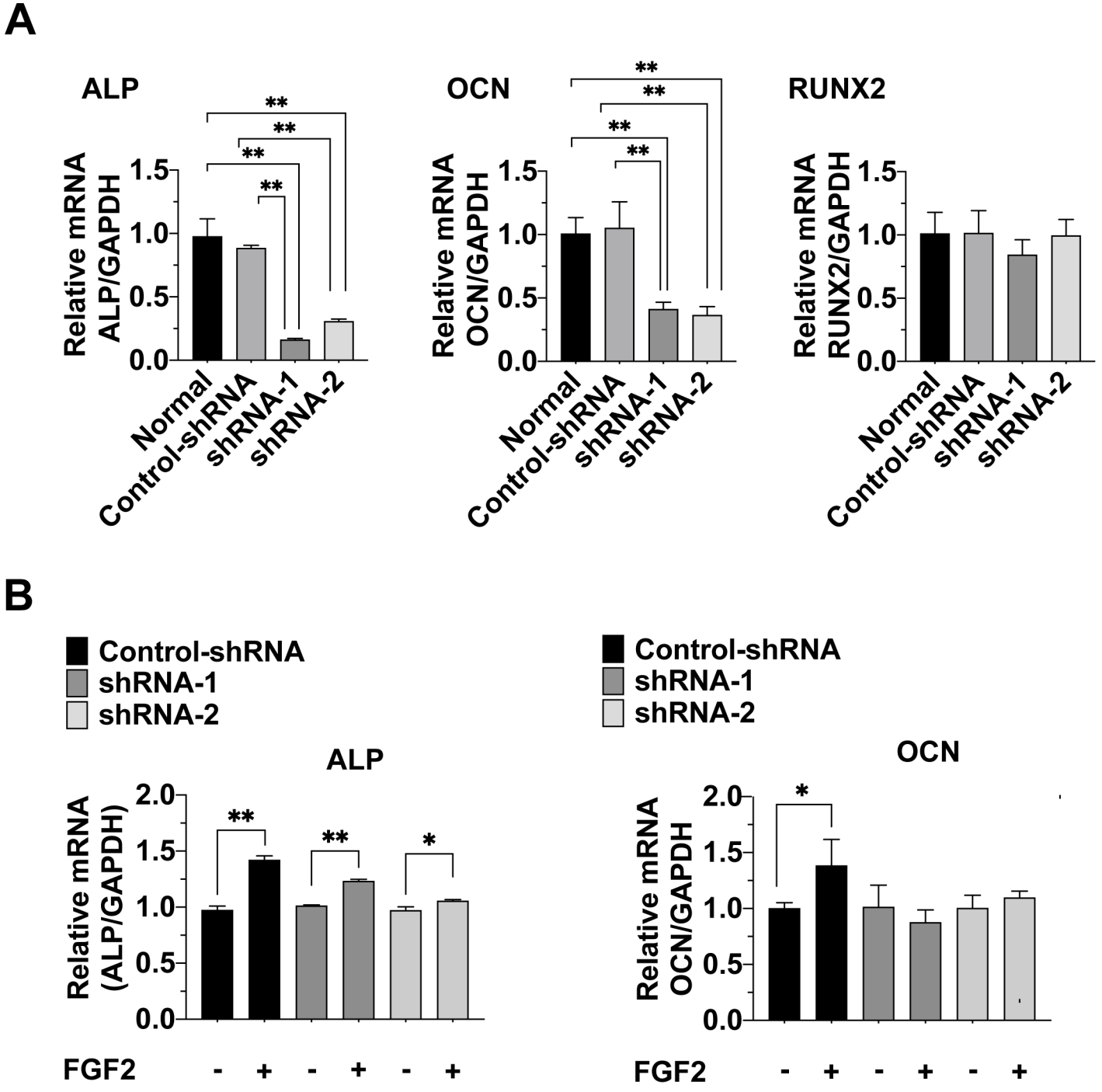
A
ALP
OCN
RUNX2
Relative mRNA ALP/GAPDH
Relative mRNA OCN/GAPDH
Relative mRNA RUNX2/GAPDH
1.5
1.0
0.5
0.0
**
Normal
Control-shRNA
shRNA-1
shRNA-2
B
Control-shRNA
shRNA-1
shRNA-2
ALP
OCN
Relative mRNA (ALP/GAPDH)
Relative mRNA OCN/GAPDH
2.0
1.5
1.0
0.5
0.0
*
FGF2
- + - + - +

Figure 4

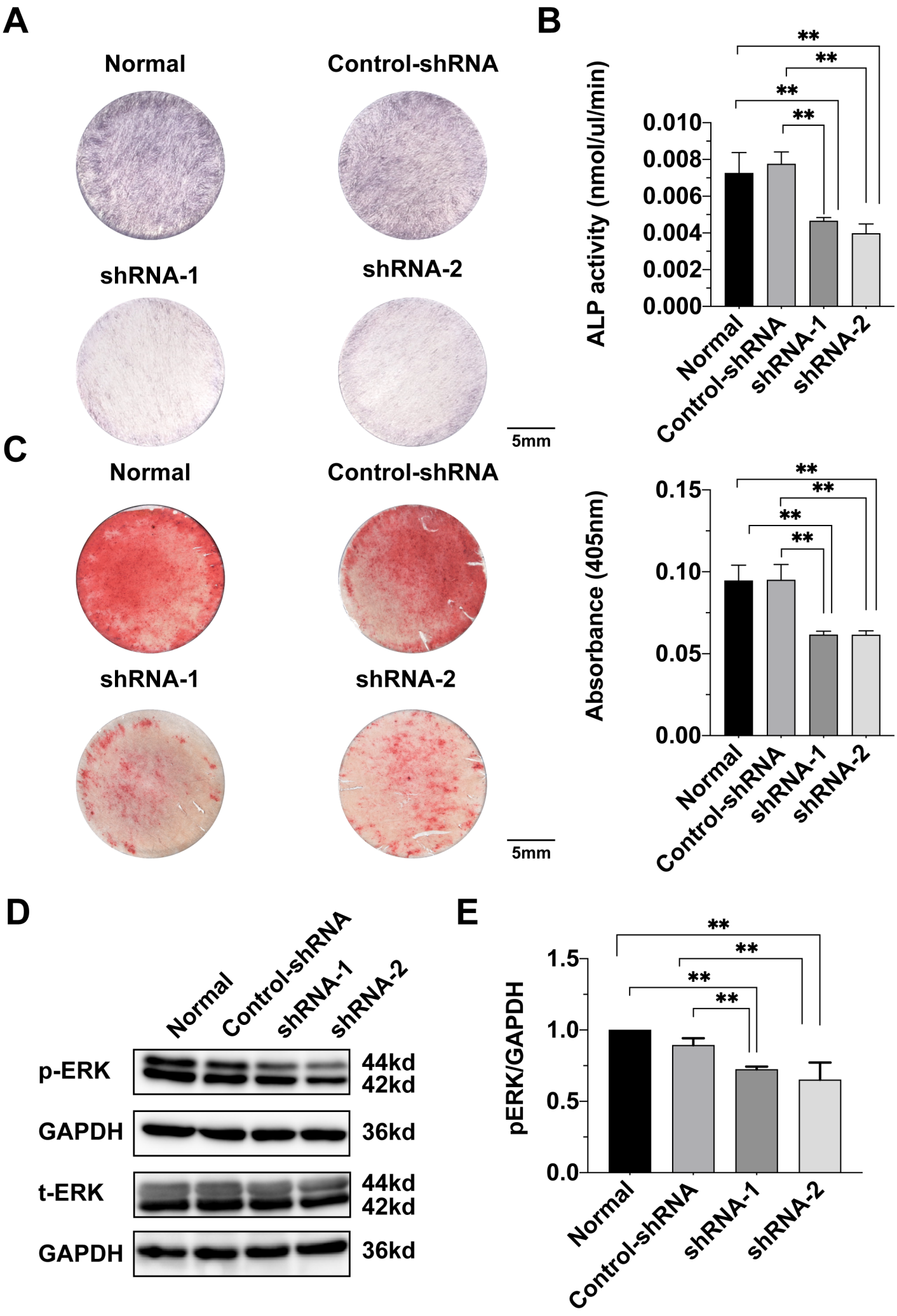
A
Normal
Control-shRNA
shRNA-1
shRNA-2
5mm
B
ALP activity (nmol/ul/min)
0.010
0.008
0.006
0.004
0.002
0.000
**
Normal
Control-shRNA
shRNA-1
shRNA-2
C
Normal
Control-shRNA
shRNA-1
shRNA-2
5mm
Absorbance (405nm)
0.15
0.10
0.05
0.00
D
Normal
Control-shRNA
shRNA-1
shRNA-2
p-ERK
44kd
42kd
GAPDH
36kd
t-ERK
44kd
42kd
GAPDH
36kd
E
pERK/GAPDH
1.5
1.0
0.5
0.0

Figure 5

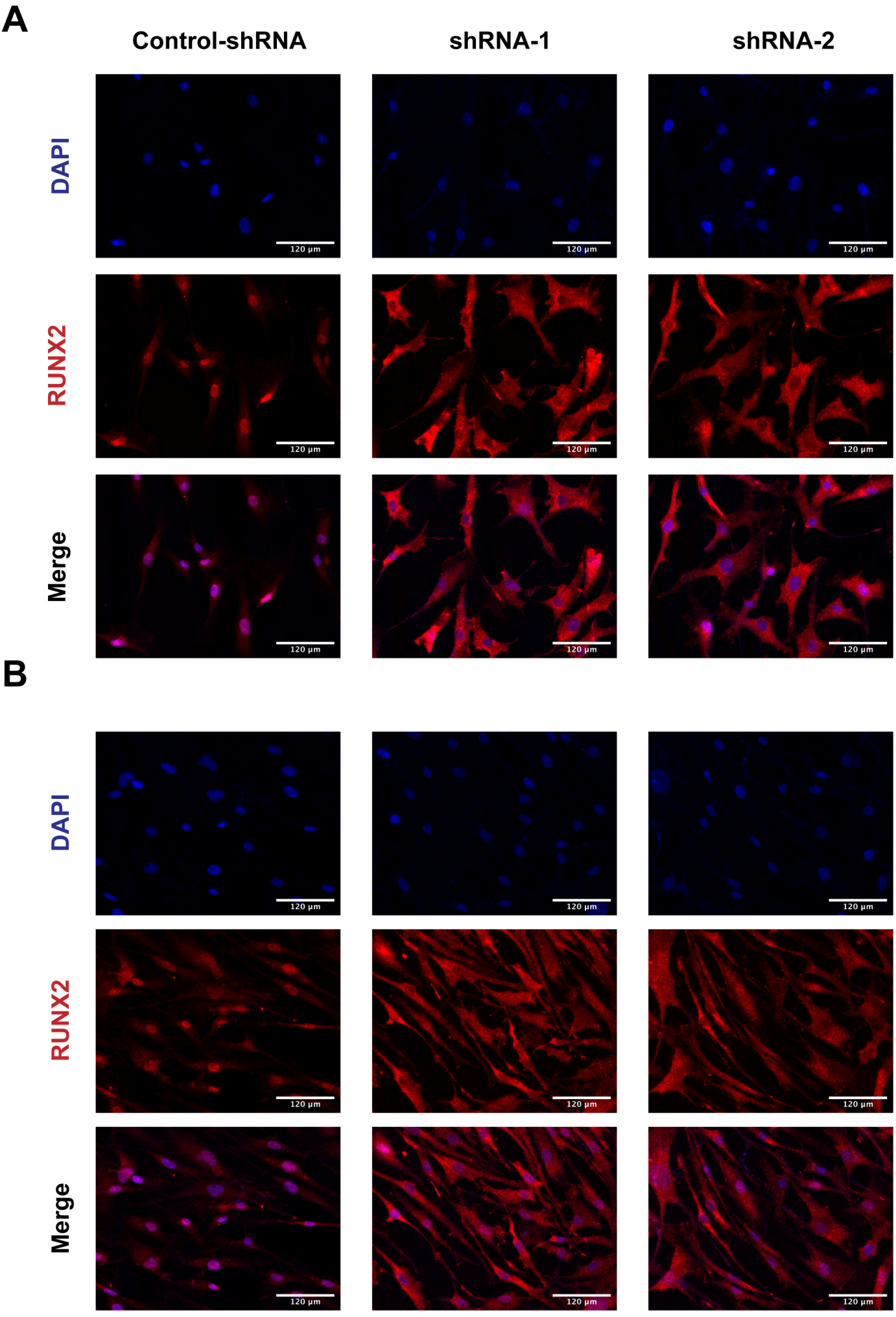
A
Control-shRNA
shRNA-1
shRNA-2
DAPI
RUNX2
Merge
120 μm
B
DAPI
RUNX2
Merge
120 μm

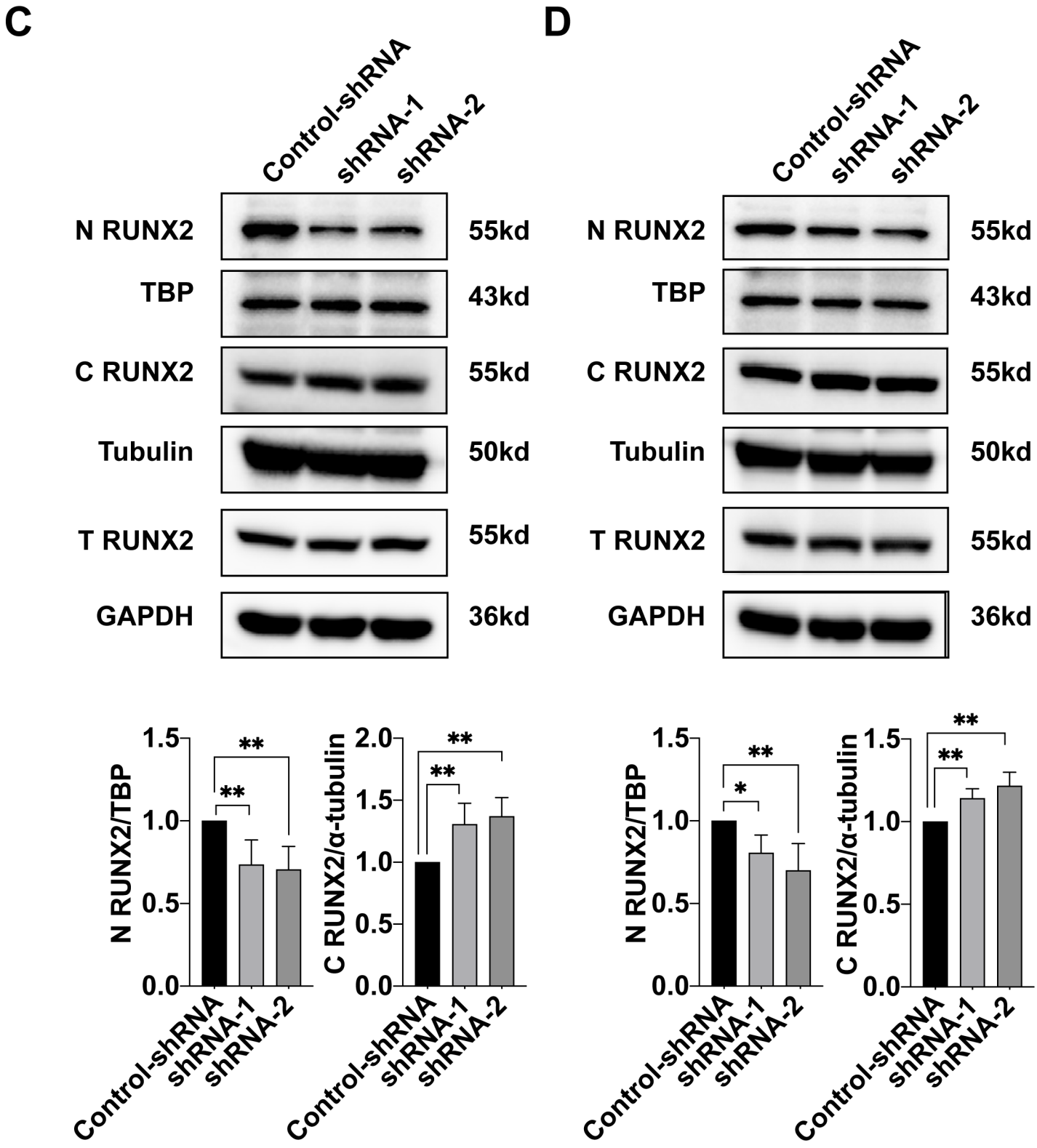
C
Control-shRNA
shRNA-1
shRNA-2
N RUNX2
55kd
TBP
43kd
C RUNX2
55kd
Tubulin
50kd
T RUNX2
55kd
GAPDH
36kd
N RUNX2/TBP
1.5
1.0
0.5
0.0
**
**
Control-shRNA
shRNA-1
shRNA-2
C RUNX2/α-tubulin
2.0
1.5
1.0
0.5
0.0
**
**
Control-shRNA
shRNA-1
shRNA-2
D
Control-shRNA
shRNA-1
shRNA-2
N RUNX2
55kd
TBP
43kd
C RUNX2
55kd
Tubulin
50kd
T RUNX2
55kd
GAPDH
36kd
N RUNX2/TBP
1.5
1.0
0.5
0.0
*
**
Control-shRNA
shRNA-1
shRNA-2
C RUNX2/α-tubulin
1.5
1.0
0.5
0.0
**
**
Control-shRNA
shRNA-1
shRNA-2

Figure 6

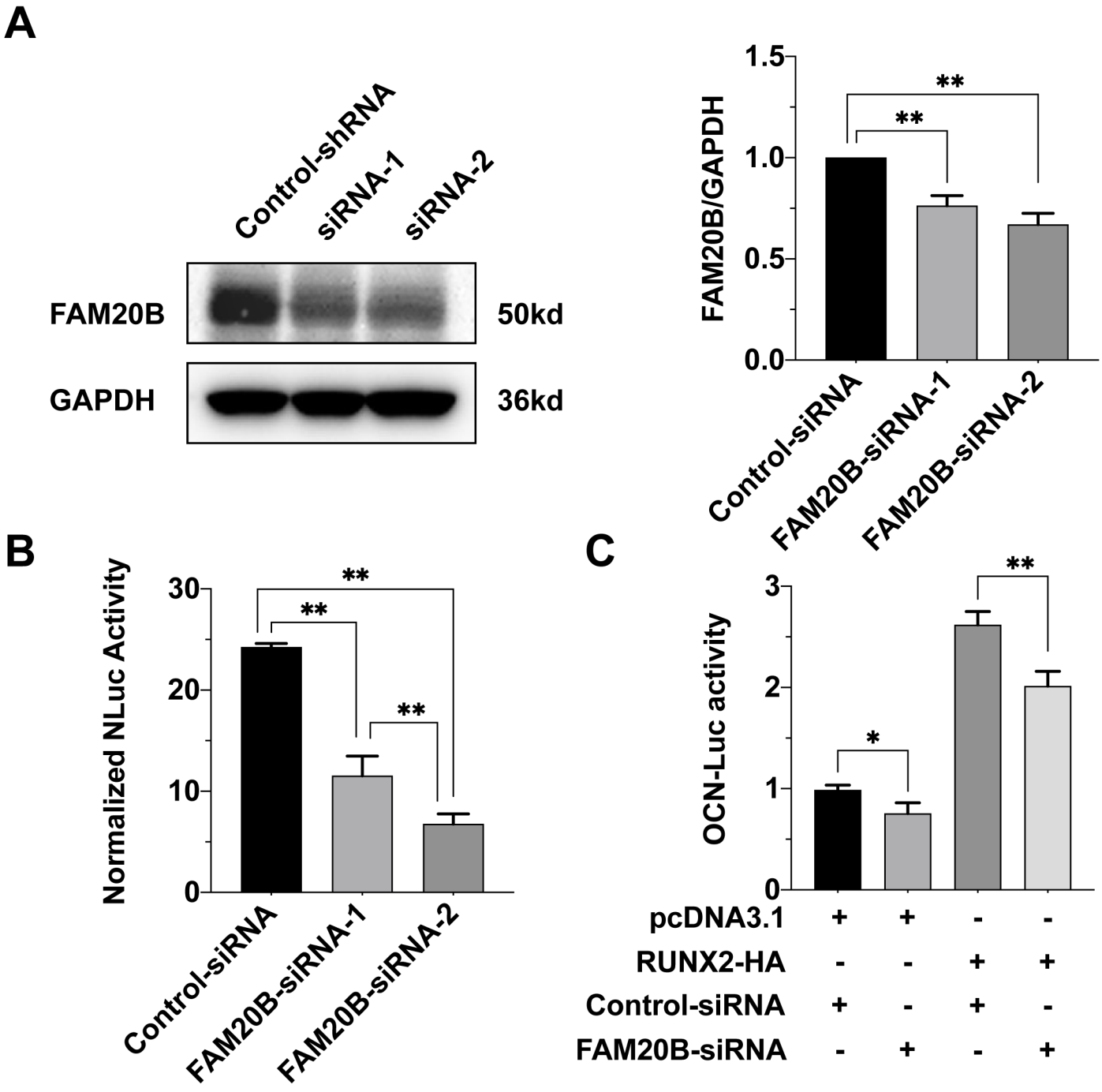
A
Control-shRNA
siRNA-1
siRNA-2
FAM20B
50kd
GAPDH
36kd
FAM20B/GAPDH
1.5
1.0
0.5
0.0
**
**
Control-siRNA
FAM20B-siRNA-1
FAM20B-siRNA-2
B
Normalized NLuc Activity
30
20
10
0
**
**
**
Control-siRNA
FAM20B-siRNA-1
FAM20B-siRNA-2
C
OCN-Luc activity
3
2
1
0
*
**
pcDNA3.1 + + - -
RUNX2-HA - - + +
Control-siRNA + - + -
FAM20B-siRNA - + - +